Journal of proteome research

Article

pubs.acs.org/jpr

Metabolomic Analysis of Akt1-Mediated Muscle Hypertrophy in Models of Diet-Induced Obesity and Age-Related Fat Accumulation

Kian-Kai Cheng,[†,‡] Yuichi Akasaki,[§,∥] Emmanuelle Lecommandeur,[†] Ross T. Lindsay,[†] Steven Murfitt,[†] Kenneth Walsh,[§] and Julian L. Griffin*[,†,⊥]

[†]Department of Biochemistry and Cambridge Systems Biology Centre, University of Cambridge, Cambridge CB2 1GA, United Kingdom

[‡]Department of Bioprocess Engineering and Innovation Centre in Agritechnology, Universiti Teknologi Malaysia, Johor Bharu, Johor 81310, Malaysia

[§]Molecular Cardiology, Whitaker Cardiovascular Institute, Boston University School of Medicine, Boston, Massachusetts 02118, United States

[∥]Department of Cardiovascular Medicine and Hypertension, Graduate School of Medical and Dental Sciences, Kagoshima University, Kagoshima 890-8520, Japan

[⊥]Elsie Widdowson Laboratory, Medical Research Council (MRC) Human Nutrition Research, Cambridge CB1 9NL, United Kingdom

Supporting Information

ABSTRACT: Akt1 is a serine/threonine kinase that promotes cell growth and survival. Previously, Akt1 activation in a double transgenic (DTG) mouse model fed a high-fat/high-sucrose (HF/HS) diet was found to promote type IIb muscle growth and to lead to a significant reduction in obesity. Here, we have used metabolomics to examine the metabolic perturbations in blood serum and liver and gastrocnemius tissues of the DTG mice. Multivariate statistics highlighted consistent metabolic changes in gastrocnemius muscle following Akt1 activation, which included significant reductions of serine and histidine-containing dipeptides (anserine and carnosine), in addition to increased concentrations of phosphorylated sugars. In addition, Akt1-mediated regression in obesity could be associated with increased glycolysis in gastrocnemius muscle as well as increased gluconeogenesis, glycogenolysis, and ketogenesis in the liver. In old DTG animals, Akt1 activation was found to improve glucose metabolism and confer a beneficial effect in the regression of age-related fat accumulation. This study identifies metabolic changes induced by Akt1-mediated muscle growth and demonstrates a cross-talk between distant organs that leads to a regression of fat mass. The current findings indicate that agents that promote Akt1 induction in muscle have utility in the regression of obesity.

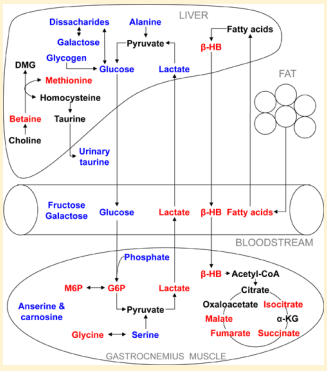

KEYWORDS: *Protein kinase B, metabonomics, obesity, type 2 diabetes*

INTRODUCTION

Akt, or protein kinase B, is a protein from the serine/threonine kinase family that is involved in signaling during cell growth and proliferation, apoptosis, transcription, angiogenesis, migration, and glucose metabolism.[1−4] Increased Akt activity has been found in numerous cancer types, but the loss of Akt activation has been associated with the development of type-2 diabetes, suggesting that the Akt pathway is an attractive therapeutic target for these diseases.[2−4] Akt is a downstream component in phosphoinositide 3-kinase (PI3K) signaling, and it is activated by a wide range of stimuli, including insulin and insulin-like growth factor.[1] The downstream kinase targets of Akt include glycogen synthase kinase 3, mammalian target of rapamycin (mTOR), $p70^{S6K}$, PHAS-1 (4EBP-1), and the Foxo family, demonstrating the important role Akt plays in regulating metabolism.[5]

To date, three Akt isoforms have been identified in mammals, namely, Akt1, Akt2, and Akt3 (also known as PKBα, PKBβ, PKBγ, respectively).[4] Akt1 is known to be involved in cell growth, but recent studies have also demonstrated its role in energy metabolism, suggesting that it is a potential target in treating obesity.[6,7] Previously, we have described a double transgenic (DTG) mouse model with inducible Akt1 expression in skeletal muscle.[6,8] Muscle-specific Akt1 overexpression was found to selectively induce type IIb muscle hypertrophy, improve insulin sensitivity, and cause reductions in fat mass and blood glucose concentration. In addition, transcriptomics indicated increased glycolysis in the gastrocnemius muscle as well as upregulated gluconeogenesis and ketogenesis in the liver of the DTG animals.

In the current study, we have used a combination of proton nuclear magnetic resonance (^{1}H NMR) spectroscopy, gas

Special Issue: Environmental Impact on Health

Received: July 19, 2014
Published: September 18, 2014

chromatography−mass spectrometry (GC−MS), GC with a flame ionization detector (GC−FID), and liquid chromatography−mass spectrometry (LC−MS) to investigate the metabolic perturbations in blood serum and liver and gastrocnemius tissues of the DTG mice. We then placed these metabolic changes in the context of Akt1 induction and the subsequent conferred metabolic advantage in terms of reducing obesity and reducing insulin resistance in aged animals. Our results identified pathways that were perturbed by Akt1 activation, leading to regression of diet-induced obesity and improvement of age-related fat accumulation. In addition, a metabolomic study of the gastrocnemius muscle identified a metabolic signature of Akt1 overexpression, which was also observed in models of obesity and advanced age.

MATERIAL AND METHODS

Animals and Experimental Design

The generation of a skeletal muscle-specific, inducible Akt1 DTG mouse model has been previously described in detail.[6] In brief, 1256 [3Emut] MCK-rtTA transgenic mice[9] were crossed with TRE-myrAkt1 transgenic mice[10] to produce the DTG mouse model. In the current study, 1256 [3Emut] MCK-rtTA single transgenic mice were used as controls. All protocols were approved by the Boston University Institutional Animal Care and Use Committee.

Two studies were conducted to examine the effect of a high-fat/high-sucrose (HF/HS) diet and aging on Akt1 activation in the DTG mice. In the study on the effect of diet, 12-week old male controls and DTG mice were fed either a standard chow (Harlan Teklad global 18% protein rodent diet, no. 2018) or HF/HS (Bio-Serv, no. F1850) diet for 3 months (12 weeks; $n = 6$ for each group). Doxycycline was administered through the drinking water to all animals from weeks 9−12 of the experiment, which caused a muscle-specific Akt1 induction in the DTG mice but not in the single transgenic controls. Blood serum samples were collected before and after doxycycline administration (at weeks 8 and 12), while gastrocnemius muscle and liver tissues were collected at 3 months.

In the second study, which focused on the effect of aging, the male single transgenic controls and DTG mice (3 and 18 months old) were fed the chow diet together with doxycycline administration for 4 weeks ($n = 6$ for each group) before the samples (serum, gastrocnemius muscle, and liver tissue) were collected. All samples were stored at −80 °C until further analysis by metabolomics.

Metabolic Profiling Using ^{1}H NMR Spectroscopy

Blood serum was analyzed using a two-tube NMR system, where sodium-3-(trimethylsilyl)-2,2,3,3-tetradeuteriopropionate (TSP) was used as chemical shift standard.[11] Eighty microliters of blood serum was loaded into a capillary tube (1.7 mm o.d.) (New Era, Vineland, NJ, USA), which was then inserted into an outer 5 mm NMR tube containing 600 μL of D_2O with 0.9% w/v sodium chloride and 0.1 mM TSP (Cambridge Isotope Laboratories Inc., Andover, MA, USA) and then subsequently analyzed. For tissues, metabolites were extracted using methanol/chloroform/water extraction.[12,13] In detail, frozen tissues (~20 mg for gastrocnemius muscle and ~40 mg for liver tissue) were first transferred into microcentrifuge tubes (Starlab, UK). Then, a stainless steel bead was added to each tube, followed by 600 μL of chloroform/methanol (2:1) (both from Sigma-Aldrich). Tissues were then homogenized using a TissueLyser (Qiagen, UK), and the resulting homogenates were sonicated for 15 min. The stainless steel beads were removed, and chloroform and water (200 μL of each) were added to each tube before the samples were centrifuged at 13 300 rpm for 10 min. After that, the aqueous and organic phases were separated from the protein pellets. The aqueous phase was dried using an evacuated centrifuge (Eppendorf, Hamburg, Germany), while the organic phase was evaporated to dryness in a fume hood. All dried samples were stored at −80 °C until further analysis. Prior to ^{1}H NMR analysis, dried tissue extracts were dissolved in 600 μL of D_2O containing TSP (0.5 mM for the extracts of liver tissue or 0.2 mM for the extracts of gastrocnemius muscle) and sodium azide (~0.1% w/v).

The blood serum and tissue extracts were analyzed by ^{1}H NMR spectroscopy at 500 MHz at 300 K for tissue extracts and at 310 K for blood serum, using a solvent suppression pulse sequence based on a one-dimensional NOESY pulse sequence. The NMR spectra were processed using ACD SpecManager 1D NMR processor (version 8, ACD, Toronto, Canada). Spectra were Fourier-transformed, referenced to TSP at 0.0 ppm, and were phased and baseline-corrected manually. Each spectrum was integrated using 0.02 ppm integral regions between 0.2 and 10.0 ppm for tissue spectra and −0.04 and 10.0 ppm for serum spectra. The water-containing region (4.7−4.8 ppm for tissue spectra and 4.5−5.0 ppm for serum spectra) was excluded from further analysis. Each integral region of blood serum NMR spectra was normalized to the integral value of TSP for each spectrum. To account for any difference in concentration between tissue samples, each spectral region was normalized to a total integral value of 1. All NMR peaks were assigned on the basis of the Human Metabolome database[14] (http://www.hmdb.ca), published literature,[15] Chenomx NMR suite version 5.1 (Chenomx, Alberta, Canada), or by the use of authentic standards.

Metabolic Profiling Using Gas Chromatography

Prior to GC−MS analysis, L-proline (U-$^{13}C_5$, 98%), L-glutamic acid (U-$^{13}C_5$, 98%; ^{15}N, 98%), and myristic acid (1,2,3-$^{13}C_3$, 99%) (Cambridge Isotope Laboratories Inc., Andover, MA, USA) were added to the aqueous soluble metabolites as internal standards, and the sample was dried using an evacuated centrifuge (Eppendorf, Hamburg, Germany). The dried samples were then derivatized using a two-step procedure.[16] First, the samples were methoxymated using 30 μL of methoxyamine hydrochloride (20 mg/mL in pyridine; Sigma-Aldrich Ltd., Dorset, UK) for 17 h. Then, the samples were silylated using 30 μL of *N*-methyl-*N*-trimethylsilyltrifluoroacetamide (MSTFA; Macherey-Nagel, Duren, Germany) for 1 h at room temperature. The derivatized samples were then diluted with hexane (200 μL final volume) and analyzed using a Trace GC Ultra coupled to a DSQ II single-quadrupole mass spectrometer (ThermoScientific, Hemel Hempstead, UK). The column used was 5% polysilarylene, 95% polydimethylsiloxane (30 and 0.25 mm i.d.) (Phenomenex, Macclesfield, Cheshire, UK). During data acquisition, the temperature was ramped from 70 to 310 °C in a 35 min period. The resulting mass spectra were matched to the National Institute of Standards and Technology (NIST) library. Overlapping peaks were deconvoluted using traces of selected ions.

To profile the total fatty acid complement of blood plasma and the tissue extracts, organic soluble metabolites were derivatized using an acid-catalyzed esterification procedure.[17] Specifically, dried organic soluble metabolites were dissolved in 750 μL of chloroform/methanol (1:1) and transferred into a glass vial. Then, 250 μL of boron trifluoride (BF_3; 10% in methanol; Sigma-Aldrich) was added, and the samples were incubated at 80 °C for 90 min. The derivatized samples were then analyzed

dx.doi.org/10.1021/pr500756u | J. Proteome Res. 2015, 14, 342−352

using a Focus GC, and the column eluent was introduced into a flame-ionization detector (FID, Thermo Electron Corporation). The column used was a TR-FAME column (30 m × 0.25 mm i.d.) with a 70% cyanopropyl polysilphenylene-siloxane stationary phase (ThermoScientific). During the experiment, the temperature was ramped from 55 to 230 °C in a 28 min run. Assignment of organic phase metabolites was carried out by comparison with a FAME standard mix (Supelco 37 Component FAME Mix; Sigma-Aldrich) and mass spectrometry where necessary.

For both aqueous and organic phase metabolites analysis, the GC chromatograms were processed using Xcalibur (version 2.0; ThermoScientific), in which each individual peak was integrated manually and then normalized to the internal standard peak(s).

Lipidomics by Liquid Chromatography–Mass Spectrometry

Analysis was performed using a Waters Xevo G2 quadrupole time-of-flight mass spectrometer (Waters Ltd., Hertfordshire, UK) with an electrospray ionization probe and a Z-spray ion source. The spectrometer was coupled to a Waters Acquity UPLC system.

One-fifth of the organic fractions of gastrocnemius and liver tissue was dissolved in 100 μL of 1:1 methanol/chloroform. The resulting lipid solution was further diluted with 900 μL of 2:1:1 *iso*-propanol/acetonitrile/water containing 20 μM phosphotidylcholine (PC 34:0) (Avanti Polar Lipids, CA, USA) as an internal standard and placed inside a 1.5 mL glass screwtop vial (Agilent, Santa Clara, CA, USA) and capped for analysis. Ten microliters of each sample was combined into a new vial and used as a pool sample for quality control and analyte identification. All analyses were conducted using a method utilizing simultaneous low- and high-energy mass scan functions in both negative and positive ionization modes to provide fragmentation data for lipid identification. Both functions used a centroid full scan from 50 m/z to 1200 m/z with a capillary voltage and cone voltage of 3.0 kV and 30 V for positive ion mode and 2.5 kV and 25 V for negative ion mode, respectively. Compounds were separated using a CSH C18 column (2.1 mm × 100 mm, 1.7 μm; Waters Ltd., Hertfordshire, UK). Mobile phase A consisted of 10 mM ammonium formate in 3:2 acetonitile/water, and mobile phase B consisted of 10 mM ammonium formate in 9:1 *iso*-propanol/acetonitrile. The chromatography gradient was as follows: a linear gradient of 40 to 43% B over 2.0 min followed by an increase to 50% B over 0.1 min and then to 54% until 12.0 min. The composition of B was then increased to 70% over the following 0.1 min and further increased to 99% until 18 min, at which time the column was equilibrated for 2 min to give a total run time of 20 min. The flow rate was 400 μL/min, and the column temperature was 55 °C. The injection volume was 5 μL.

Data were processed using MarkerLynx within the software suit Masslynx (version 1.4) by Waters Ltd. (Herfordshire, UK). Peak areas were collated and normalized in Excel (Microsoft). All spectral peak areas were normalized against the total area of all peaks within a sample. Lipid species were identified by fragmentation data obtained from the high-energy function described above and compared with online databases (e.g., www.lipidmaps.org).

Statistical Data Analysis

Data sets were imported into SIMCA-P+ 11.0 (Umetrics, Umeå, Sweden) for processing using principal components analysis (PCA), partial least-squares (PLS) analysis, and PLS-discriminant analysis (PLS-DA) (a regression extension of PCA used for classification). Prior to multivariate analysis, the NMR and LC–MS data sets were mean-centered and Pareto-scaled, while the GC–MS and GC–FID data sets were mean-centered and scaled to unit variance. Pareto scaling weights each variable with the square root of its standard deviation and therefore increases the weighting of low-intensity metabolites while at the same time limiting the influence of noise on the multivariate model. Unit variance scaling weights each variable with its standard deviation, and the resulting model is not biased toward high-concentration metabolites.

The Q^2 and R^2 values from the resulting multivariate model were used to assess the robustness of a model, where R^2 shows the fraction of variation explained by a component, and Q^2 shows the predictability of the model through cross-validation. Typically, a robust model has a $Q^2 > 40\%$. In addition, these models were assessed for robustness using the validation tool within SIMCA that assesses the Q^2 and R^2 for each model against models produced, where the Y value for class membership has been permuted to produce random models. Here, a robust model is represented by $Q^2_{\text{actual}} \gg Q^2_{\text{random}}$.

Identification of major metabolic perturbations within the pattern recognition models was achieved by analysis of corresponding loadings plots. In addition, the differential metabolites found were confirmed by standard univariate tests (for example, Student's t-test).

RESULTS

Akt1-Induced Muscle Hypertrophy Reduced Both Diet-Induced and Age-Related Fat Accumulation

To place our subsequent metabolomics studies in a physiological context, we first investigated the effect of Akt1 overexpression on diet-induced obesity. Twelve-week old mice were fed either a normal chow or HF/HS diet for 8 weeks before Akt1 gene induction. The HF/HS diet caused an increase in body weight for both the controls and DTG mice (Figure 1A). As previously reported, the overall weight gain was significantly less in the DTG animals following 4 weeks of Akt1 activation ($p < 0.05$), whereby the controls showed a further increasing trend in body weight (Figure 1A). In contrast, Akt1 gene induction had no effect on body weight for mice fed a normal chow diet.

Next, we examined the effect of Akt1 overexpression on the weight of tissues in the same animals after 4 weeks of Akt1 activation. Akt1 induction caused a 34.8% increase in gastrocnemius muscle weight, and the extent of muscle growth did not depend on the dietary conditions used in the current study (Figure 1B, right). Compared with HF/HS-fed controls, the inguinal and subcutaneous fat masses of the HF/HS-fed DTG mice were 49.0 and 59.7% lower, respectively (Figure 1B, left and middle, $p < 0.01$). Similarly, the DTG mice fed the normal diet also showed a reduction in inguinal fat mass, but to a lesser extent.

To investigate the effect of aging on Akt1-mediated muscle hypertrophy, we next studied chow-fed controls and DTG mice at two different age groups (12 weeks and 18 months). Notably, in old animals, the extent of Akt1-induced muscle hypertrophy was found to be significantly less than that in the young animals (Figure 1C, right; $P = 0.0075$). In addition, aging led to fat accumulation in the old animals (Figure 1C, left and middle), and the data in the current study showed that this could be improved by Akt1 activation. As compared with the controls, the inguinal and subcutaneous fat of the old DTG animals were found to be 33.3 and 32.3% lower, respectively. The age-related fat accumulation was balanced by a decreased weight of muscle and probably other tissues, as no significant difference in total body weight was

dx.doi.org/10.1021/pr500756u | J. Proteome Res. 2015, 14, 342–352

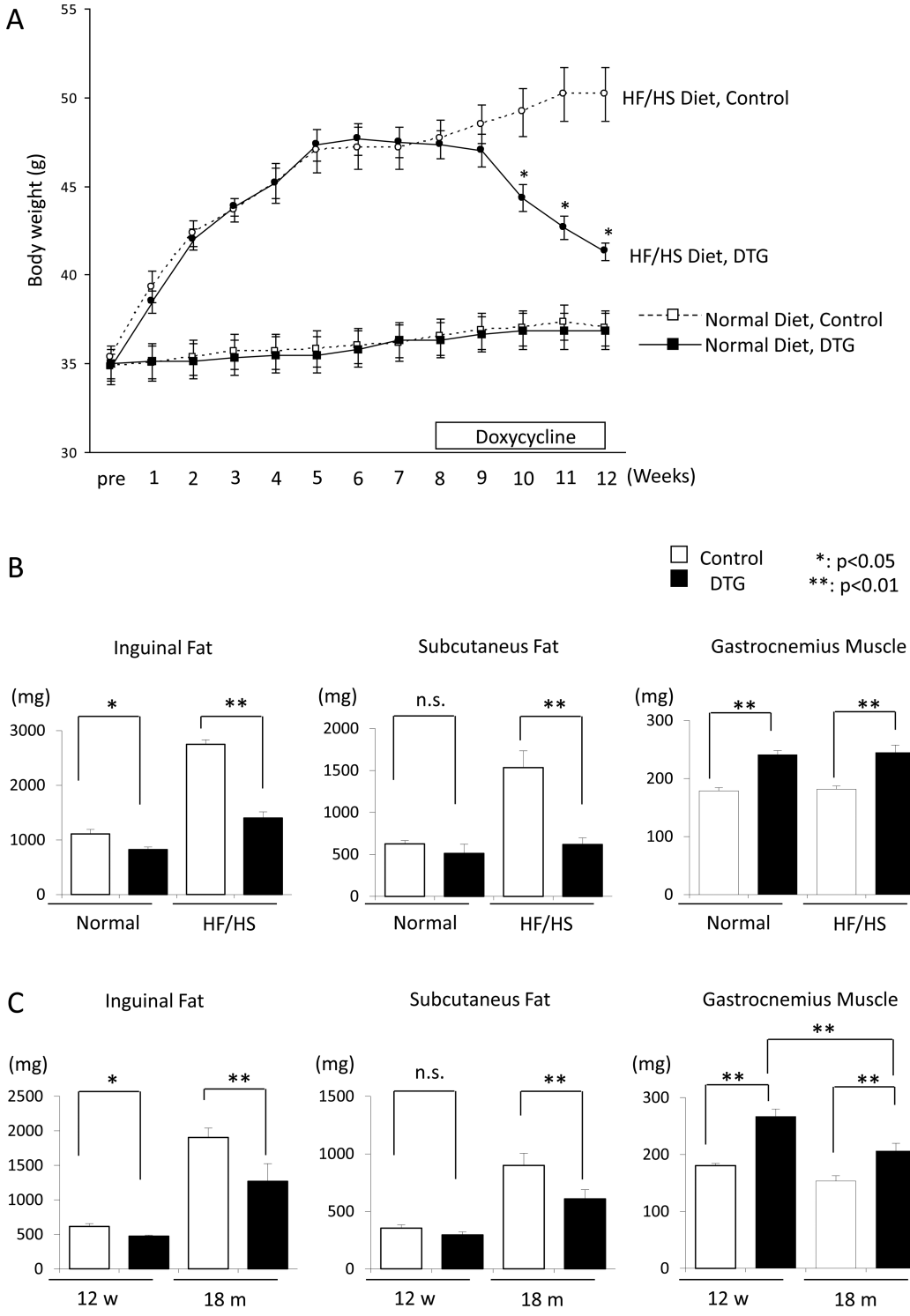

Figure 1. Obesity induced by a high-fat/high-sucrose diet could be regressed by Akt1 induction (A). The corresponding changes in tissue weight (B). Akt1 induction also conferred a reduction in age-related fat accumulation (C).

observed for all four studied groups in the aging study (Supporting Information Figure S1).

Metabolic Signature of AKT1-Induced Muscle Hypertrophy

Analysis of ^{1}H NMR data of gastrocnemius muscle (n = 48 for the total number of animals, including data from both diet and aging studies) using unsupervised PCA shows clustering of samples based on induced genotype (Supporting Information Figure S2). The result indicated that Akt1 induction is the major source of metabolic variation, suggesting potential metabolic markers for Akt1-induced muscle hypertrophy.

To further define these metabolic changes, the data were analyzed using PLS-DA to assess the discrimination between the single transgenic controls and DTG mice. This supervised analysis produced a robust two-component model (Figure 2A), which was validated using a permutation test within SIMCA P+ (Figure 2B). The most discriminatory compounds identified by the analysis were anserine and carnosine (assigned by the spiking

dx.doi.org/10.1021/pr500756u | J. Proteome Res. 2015, 14, 342−352

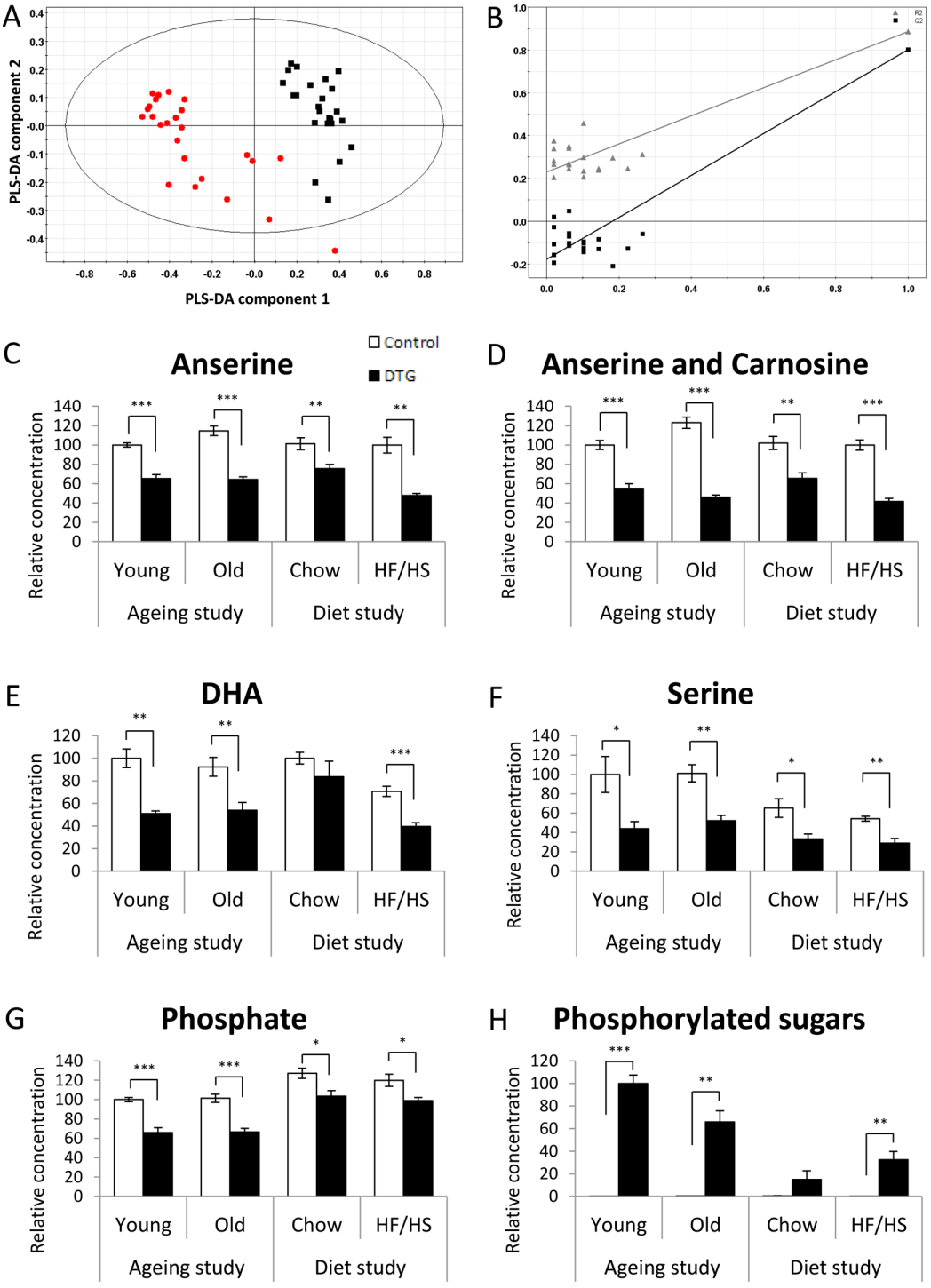

Figure 2. PLS-DA scores plot of the NMR spectra of gastrocnemius muscle tissue show separation between the controls (black squares) and DTG (red dots) mice (R^2X = 43%, R^2Y = 75%, Q^2 = 72%, for the first component) (A). Satisfactory cross-validation plot for the PLS-DA model demonstrating a robust PLS-DA model (B). Changes in a number of metabolites induced by Akt1 activation were found to be consistent across both diet and aging effects: anserine (C), anserine and carnosine (D), DHA (E), serine (F), phosphate (G), and phosphorylated sugars (H). Peak areas for young controls (C−G) or young DTG mice (H) from the aging study were normalized to 100 for comparison. (*P < 0.05, ** P < 0.01, and *** P < 0.001.)

of authentic anserine and carnosine standards, Supporting Information Figure S3). After 4 weeks of Akt1 activation, there was a 39.2% average reduction in anserine (t test, $P = 2.55 \times 10^{-13}$) and 50.9% reduction in the carnosine/anserine multiplets (t test, $P = 3.28 \times 10^{-16}$) (Figure 2C,D). Analysis of an additional spectral region (7.00−7.25 ppm) where anserine and carnosine are coresonant also showed a reduction of 50.7% (t test, $P = 2.34 \times 10^{-17}$) following Akt1 activation. This result indicated that both anserine and its precursor, carnosine, were reduced by Akt transgene induction in muscle, both in young and old mice and when mice are fed either a normal or HF/HS diet.

The aqueous metabolites in the gastrocnemius muscle were also profiled using a complementary GC−MS method. Analysis by PLS-DA further identified significant reductions in inorganic

dx.doi.org/10.1021/pr500756u | J. Proteome Res. 2015, 14, 342−352

phosphate and serine as well as increased concentrations of phosphorylated sugars (including glucose-6-phosphate and mannose-6-phosphate) in the gastrocnemius muscle of the DTG mice (Figures 2F−H). In addition, GC−FID analysis also showed a reduction of docosahexaenoic acid (DHA) concentration in the muscle tissues of the DTG mice from the aging study and the HF/HS-fed DTG mice from the diet study (Figure 2E). These changes constitute the metabolic signature associated with Akt1-induced muscle hypertrophy, which are found consistently across the effects of diet and aging measured in this study.

Metabolic Perturbation Associated with Akt1-Mediated Weight Loss

One focus of this study was to elucidate the metabolic perturbations associated with the Akt1-mediated weight loss in the HF/HS-induced obese DTG mice. PLS-DA of the NMR spectra from gastrocnemius muscle showed a clear separation between the controls and the DTG mice fed the HF/HS diet ($n = 6$) after 4 weeks of Akt1 induction ($R^2X = 48\%$, $R^2Y = 93\%$, $Q^2 = 87\%$ for the first component). In addition to the above-mentioned metabolic signatures, the two genotypes fed the HF/HS diet were further discriminated by significantly increased concentrations of β-hydroxybutyrate, succinate, glycine, and lactate in the gastrocnemius muscle of the DTG mice. Furthermore, multivariate analysis of GC−MS data also indicated a perturbation in the TCA cycle, with increased concentrations of isocitrate, fumarate, and malate found in DTG mice fed the HF/HS diet (Table 1).

Table 1. Summary of Metabolic Changes Detected Following Analysis by ^{1}H NMR Spectroscopy and GC−MS[a]

samples	increased in DTG mice	decreased in DTG mice
gastrocnemius muscle	**phosphorylated sugars****	**anserine*****
	β-hydroxybutyrate*	**carnosine*****
	lactate**	**serine****
	glycine***	**inorganic phosphate***
	succinate**	
	isocitrate***	
	fumarate***	
	malate***	
blood serum	β-hydroxybutyrate*	glucose***
	lactate*	galactose**
	lipid moieties*	fructose**
liver tissue	β-hydroxybutyrate*	glucose**
	betaine*	galactose*
	methionine*	disaccharides**
		glycogen**
		lactate*
		alanine**

[a]Comparing gastrocnemius muscle, blood serum, and liver tissue from the HF/HD-fed controls and DTG mice. *P*-values were obtained from Student's *t*-test (* $P < 0.05$, ** $P < 0.01$, and *** $P < 0.001$). The metabolites shown in bold font were found to be consistently changed across the diet and aging effects.

The impact of Akt1 overexpression on the metabolome of blood serum was then examined. PLS-DA comparing the serum metabolic profiles of the controls and the DTG mice fed a chow diet failed to produce a multivariate model, indicating that there were no marked metabolic differences between these two groups. However, a robust model was produced comparing both genotypes fed the HF/HS diet ($R^2X = 73\%$, $R^2Y = 54\%$, $Q^2 = 43\%$ for the first PLS-DA component). The serum profile of the HF/HS-fed DTG mice was characterized by increased concentrations of β-hydroxybutyrate, lactate, and lipid moieties from both phospholipids and triglycerides (δ 1.24−1.30, 1.52−1.58, 1.98−2.06, 2.76−2.84, 4.22−4.28, and 5.28−5.36) (Table 1). In addition, NMR and GC−MS data highlighted marked reductions of serum glucose (Figure 3A), fructose, and galactose concentrations in the DTG mice. After 4 weeks of Akt1 activation, the HF/HS-fed DTG mice were highlighted by a >100% increase in circulatory oleate C18:1 (*cis*-9), one of the most abundant fatty acids in serum (Supporting Information Table S1).

Multivariate statistics also indicated that the metabolic impact of Akt1 induction on the liver metabolome is diet-dependent. No PLS-DA model was produced comparing both genotypes fed a chow diet. However, when fed the HF/HS diet, PLS-DA identified a number of differential metabolites, including increased concentrations of β-hydroxybutyrate, betaine, and methionine, together with significant reductions of lactate, glucose, galactose, glycogen, alanine, and disaccharides in the DTG mice (Figure 3B,C and Table 1).

The aging process caused a higher blood glucose concentration in old controls, but this was reduced to a level comparable to that of young controls following Akt1 activation (Figure 4A). This metabolic change is most likely associated with increased muscle glycolysis induced by Akt1 induction, as increased concentrations of phosphorylated sugars and lactate were also observed in the muscle of old DTG animals (Figures 2H and 4B). Consistent with the findings in the diet study, there are no significant changes in blood glucose and muscle lactate concentrations in young animals fed a chow diet, suggesting that activation of Akt1 expression improved glucose homeostasis in old animals by restoring its expression to that of young animals.

LC−MS-Based Lipidomics of Gastrocnemius and Liver Tissue

Chromatograms from extracts from the lipid fraction of liver and gastrocnemius tissues were collected in positive and negative ionization mode and processed using multivariate statistics. Comparisons were made for a single tissue type between diet and genotype. While no statistically valid model could be built for the negative ion mode data, dominated by chromatographic peaks from free fatty acids, robust models could be built for the positive ion mode data representing chromatographic peaks from phospholipids and triglycerides.

For the liver tissue data sets, no model could be built comparing the control and DTG group on the normal chow diet. However, robust models were built comparing both the control animals on chow diet and HF/HS diet (for the PLS-DA model, $R^2X = 35\%$; $R^2Y = 99\%$; $Q^2 = 79\%$, passed cross-validation by random permutation test; data not shown) and the DTG animals on chow diet and HF/HS diet (for the PLS-DA model, $R^2X = 41\%$; $R^2Y = 99\%$; $Q^2 = 81\%$, passed cross-validation by random permutation test; Figure 5A,B). In both cases, this was driven by increases in a range of triglycerides in the HF/HS group (for the DTG group: TAG(51:2), PC(43:0), TAG(51:2), PA(30:0), TAG(53:2); PA(30:1), TAG(55:10), TAG(50:2), TAG(54:2), and TAG(53:3)) and a relative reduction of phospholipids (for the DTG group: lyso-PC(17:1)). In addition, a robust model was formed between the control mice and the DTG mice on a HF/HS diet (for the PLS-DA model, $R^2X = 38\%$; $R^2Y = 99\%$; $Q^2 = 66\%$, passed cross-validation by random permutation test; Figure 5C). This model was associated with a decrease in triglycerides

dx.doi.org/10.1021/pr500756u | J. Proteome Res. 2015, 14, 342−352

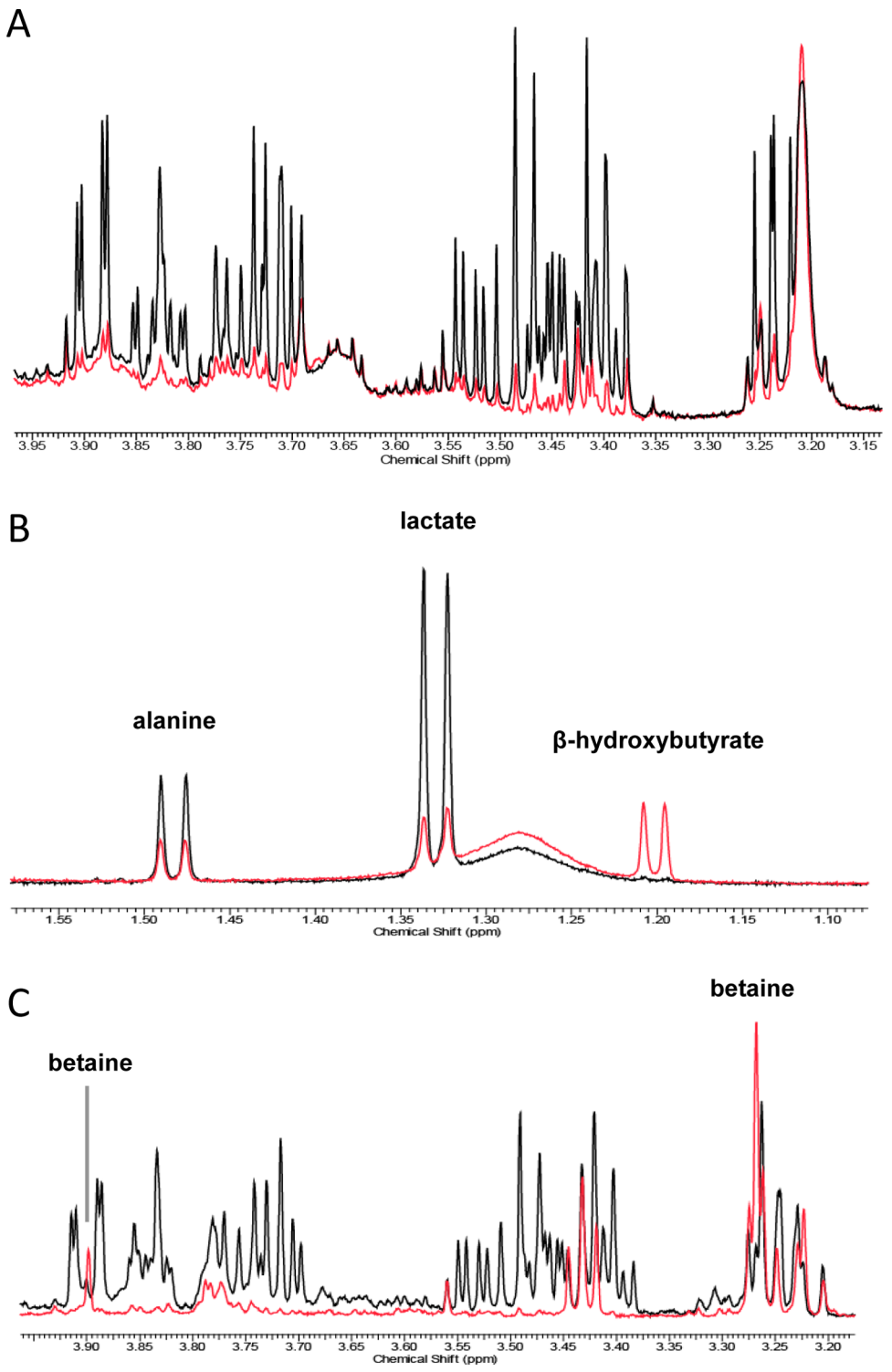

Figure 3. Multiple sections of ^{1}H NMR spectra showing (A) a marked reduction of serum glucose concentration (glucose region: δ 3.22−3.91) following Akt1 activation in HF/HS-fed mice, (B) an increased hepatic concentration of β-hydroxybutyrate and reductions of lactate and alanine in the DTG mice, and (C) an increased concentration of betaine and a marked reduction of hepatic glucose concentration (glucose region: δ 3.22−3.92) in the DTG mice. The NMR spectra were obtained from an individual sample of each class after 4 weeks of Akt1 activation: black spectrum, the HF/HS-fed controls; red spectrum, the HF/HS-fed DTG mice. Spectra were scaled to the same relative noise level.

and diacylglycerides containing longer, polyunsaturated fatty acids (TAG (53:4), TAG(56:3), and TAG(57:7)) and an increase in short chain fatty acids (TAG(48:8), TAG(50:2), TAG(46:4), TAG(48:0), TAG(47:6), TAG(48:2), and TAG(44:4)) in the DTG group.

Examining the gastrocnemius tissue, no model again could be built examining the control and DTG mice on chow diet. However, good models could be built for comparisons of the control mice on normal chow and HF/HS diets (for the PLS-DA model, $R^2X = 37\%$; $R^2Y = 99\%$; $Q^2 = 88\%$, passed cross-validation by random permutation test) and DTG mice on normal chow and HF/HS diets (for the PLS-DA model, $R^2X = 36\%$; $R^2Y = 99\%$; $Q^2 = 78\%$, passed cross-validation by random permutation

dx.doi.org/10.1021/pr500756u | J. Proteome Res. 2015, 14, 342−352

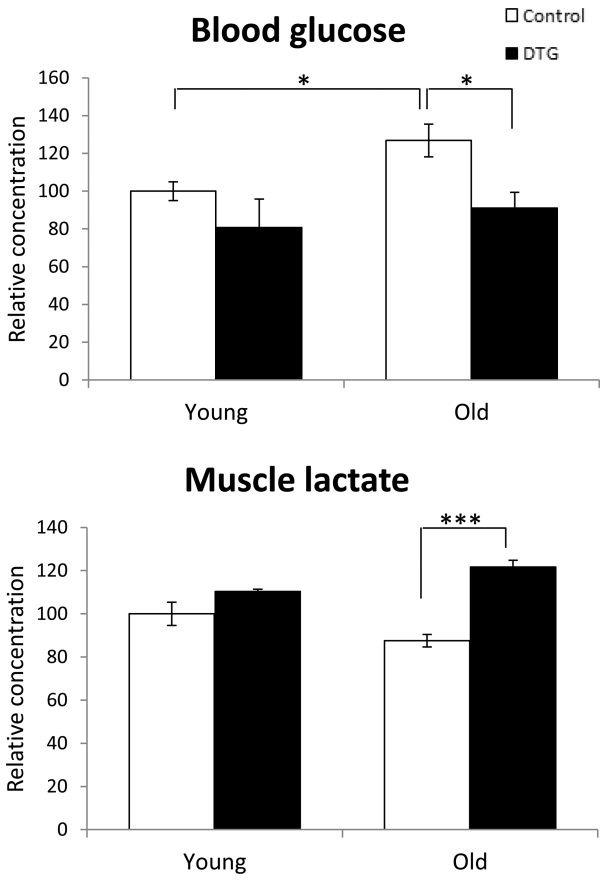

Figure 4. Increased blood glucose concentration associated with aging was reduced by Akt1 induction (A). This may be associated with increased glycolysis, as an increased concentration of lactate was detected in the hypertrophic muscle of the DTG animals (B).

test; Figure 5D,E). While a model could be built that discriminated control and DTG mice on a HF/HS diet, this did not pass cross-validation.

DISCUSSION

The increased prevalence of metabolic syndrome, obesity, and insulin resistance has led to an increased risk of cardiovascular disease in the general population.[18] Previously, a number of studies had demonstrated that induction of Akt in the skeletal muscle of mice induced muscle hypertrophy and caused a decrease in adipose tissue.[6,8,19] The reduction of fat mass following Akt1 activation was associated with enhanced lipolysis in the adipose tissue as well as an increased fatty acid oxidation in the liver.[6] These animals also exhibited improved metabolic parameters, including improved insulin sensitivity and reductions in blood glucose and leptin concentrations.

In the current study, metabolomic analysis associated Akt1 activation in mouse muscle tissue with profound metabolic perturbations in the liver, blood serum, and gastrocnemius muscle, particularly when the animals were fed a HF/HS diet (Figure 6). Notably, the HF/HS-fed DTG mice demonstrated reduced blood glucose as well as increased circulatory lactate concentration, suggesting upregulation of glycolysis following Akt1 induction in the skeletal muscle. Indeed, the examination of the metabolic composition of muscle highlighted markedly increased concentrations of glycolytic metabolites including phosphorylated sugars and lactate. This is consistent with previous findings showing increased glucose uptake and the upregulation of glycolytic genes in these animals.[6] The lactate produced via anaerobic glycolysis in muscle is transported to the liver and then metabolized to produce glucose through gluconeogenesis as part of the Cori cycle. Metabolic profiling of the liver indicated reduced lactate, alanine, and glycogen, suggesting that the liver had increased gluconeogenesis and glycogenolysis to replenish glucose stores in muscle. This cross-talk between muscle and liver enables muscle to shift its energy burden to the liver and at the same time reduce the effects of high-fat/high-sucrose feeding.

Intriguingly, the increased gluconeogenesis and glycogenolysis also stimulated fatty acid oxidation, with increased concentrations of β-hydroxybutyrate in the blood. Protein synthesis is an energy-expensive process. In the DTG mice, there was a consistent increase in the concentration of β-hydroxybutyrate in the liver, blood serum, and gastrocnemius muscle, particularly when the mice were fed the HF/HS diet. β-Hydroxybutyrate is a ketone body that is produced in the liver through ketogenesis following fatty acid oxidation. In extrahepatic tissues, it can be utilized as a fuel, being metabolized through the TCA cycle, especially during prolonged fasting or starvation.

It is known that Akt1 activation specifically induces growth of type IIb muscle fibers, also known as fast/glycolytic muscle.[6] This muscle has a lower density of mitochondria and therefore is less dependent on the TCA cycle and β-oxidation. Nevertheless, the current data demonstrated that the continuous supply of substrates in the form of ketone bodies, glucose, and possibly fatty acids led to increased concentrations of TCA cycle intermediates, including isocitrate, succinate, fumarate, and malate, in the gastrocnemius muscle of the HF/HS-fed DTG animals. This process, which involves cross-talk among muscle, liver, and adipose tissue, could serve as a supplementary energy source in addition to glycolysis for the enhanced protein synthesis needed for muscle hypertrophy.

Metabolic profiling of gastrocnemius muscle revealed a number of differential metabolites that consistently discriminated the controls and DTG mice. In the DTG mice, Akt1-induced muscle hypertrophy was associated with decreased concentrations of anserine, carnosine, inorganic phosphate, serine, and DHA, as well as increased concentrations of phosphorylated sugars in the muscle.

Among these metabolic changes, anserine and carnosine are of particular interest as they were previously reported to regulate the energy-producing pathway in proliferative tumor cells.[20,21] Carnosine (β-alanyl-L-histidine) and its methylated derivative, anserine (β-alanyl-1-methyl-L-histidine), are natural occurring histidine-containing dipeptides, which are present in many vertebrate tissues, predominantly in skeletal muscle and brain.[22] Anserine is found to be absent from human tissues despite a high concentration of carnosine (20 mM) in skeletal muscle.[23] Accumulating evidence shows that both of these dipeptides share similar structure and exhibit similar biological functions including antioxidant, pH buffering, and antiglycosylation activities, as well as metal ion chelation.[22,24] In the absence of pyruvate, carnosine and anserine are cytotoxic to transformed or tumor cells, but not to normal cells.[20] Recently, carnosine was found to inhibit ATP production through anaerobic glycolysis in cells from malignant glioma.[21] In addition, it also retards tumor growth in the N1H3T3-HER2/neu mouse model and inhibits high-glucose-induced mesangial cell proliferation.[25,26]

Increased Akt1 activity is evident in numerous cancers and proliferative cells.[27−29] In the current study, significant reductions of anserine and carnosine were associated with an upregulation

dx.doi.org/10.1021/pr500756u | J. Proteome Res. 2015, 14, 342−352

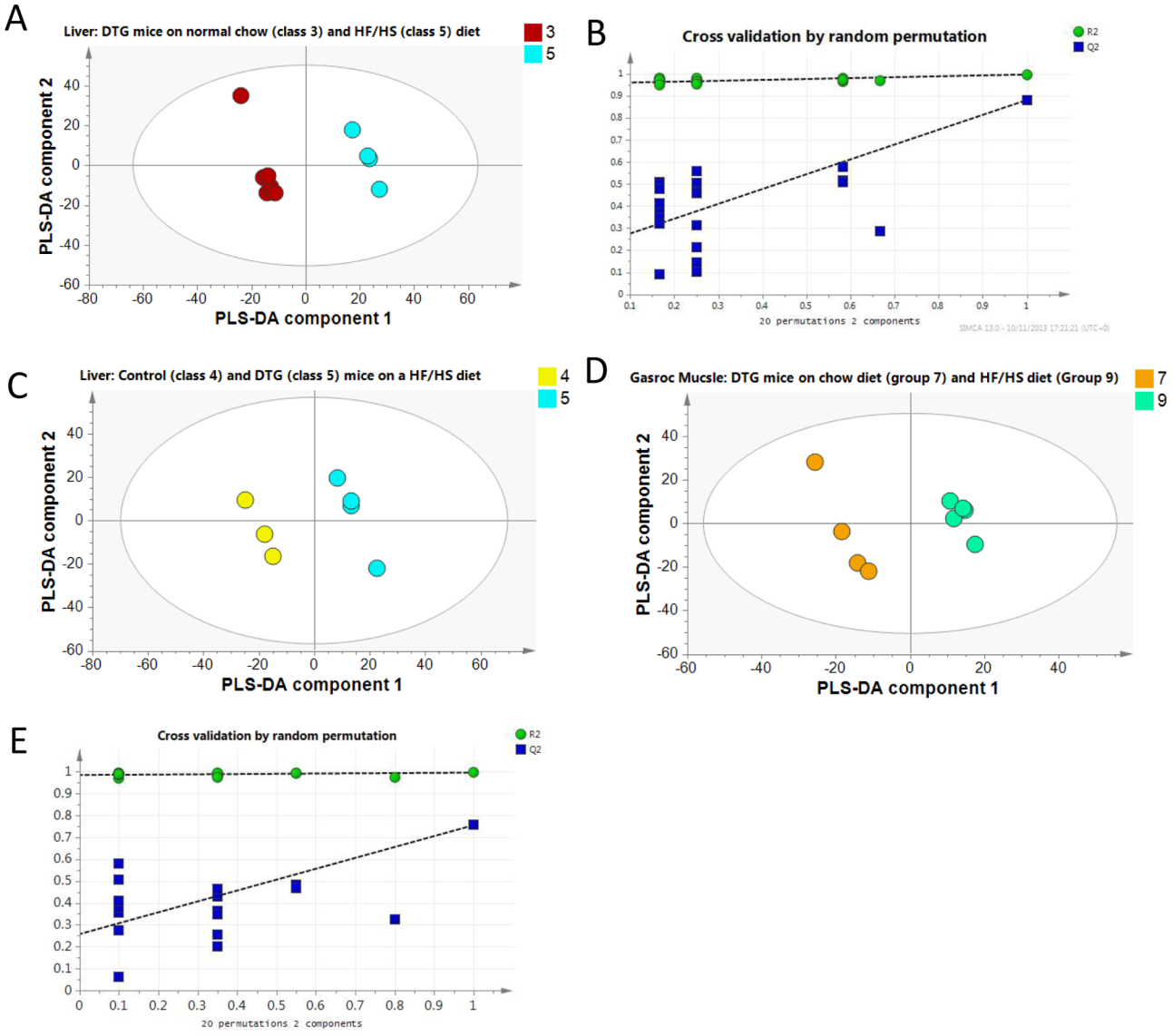

Figure 5. PLS-DA scores plot of the LC−MS lipidomic data of liver tissue show separation between DTG mice fed the chow and HF/HS diets (A). Satisfactory cross-validation plot for the PLS-DA model demonstrating a robust PLS-DA model (B). Group separation was also observed between controls and the DTG mice fed with the HF/HS diet (C). PLS-DA scores plot of the LC−MS lipidomic data of gastrocnemius tissue showed separation between DTG mice fed the chow and HF/HS diets (D); the model passed cross-validation by random permutation test (E).

in anaerobic glycolysis in gastrocnemius muscle of DTG mice. Indeed, when the mice were fed the HF/HS diet, the concentrations of these histidine-containing dipeptides were found to be negatively correlated with the lactate concentration in the gastrocnemius muscle (Figure 7). Taken together, the current findings suggest a similar regulatory role of these dipeptides on energy metabolism in Akt1-induced hypertrophic muscle and tumor cells, which both experience active cell growth and depend on ATP obtained from glycolysis.

In addition to the metabolic advantage of Akt1 induction in regulating fat accumulation induced by both diet and aging, the current study also demonstrated the beneficial effect of Akt1 in glucose homeostasis. In mice fed a HF/HS diet, the circulatory glucose concentration was reduced following Akt1 activation. Similarly, Akt1 activation was also found to reduce the increase in glucose concentration caused by aging in old animals. These results suggest an underappreciated role of Akt1 in regulating glucose metabolism.

Previously, we have shown that muscle-specific overexpression of Akt1 in the DTG mice led to an increase in circulating fibroblast growth factor 21 (FGF-21).[30] In fact, a number of metabolic perturbations observed in the current study could be associated with the metabolic role of FGF-21. FGF-21 is known to be induced by fasting and is associated with upregulated hepatic fatty acid oxidation and ketogenesis and improvement in hepatic steatosis.[31] Correspondingly, in our study, the concentration of β-hydroxybutyrate was found to be significantly increased in liver, blood serum, and gastrocnemius muscle of the DTG mice, especially when the mice were fed the HF/HS diet. This was also apparent in the LC−MS data sets from the liver tissue. While HF/HS feeding increased a range of triglycerides in the liver for both the control and DTG mice compared with animals on the chow diet, the induction of AKT led to a remodeling of the lipid species present in the liver with a reduction in longer chain polyunsaturated fatty acids and a relative increase in shorter fatty acids. Long chain polyunsaturated fatty acids are largely dietary derived, while short chain,

dx.doi.org/10.1021/pr500756u | J. Proteome Res. 2015, 14, 342−352

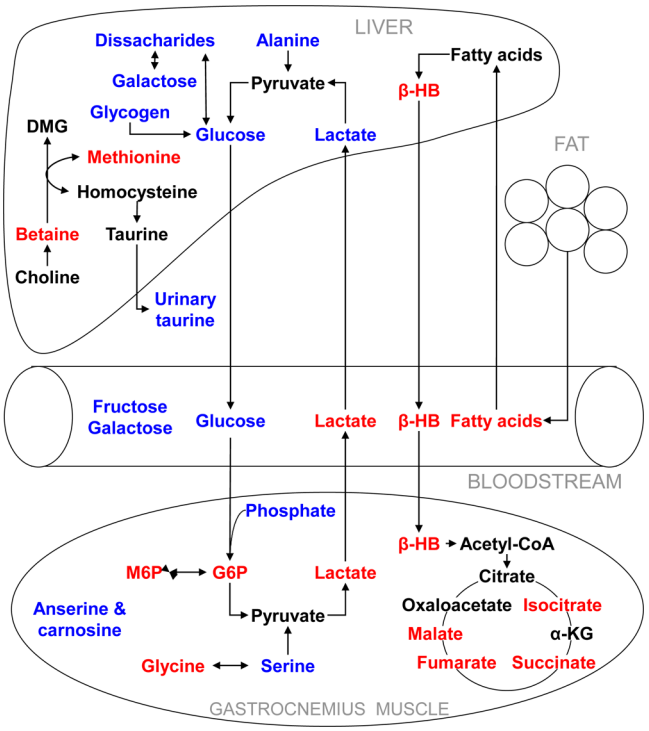

Figure 6. Profound metabolic perturbation as a result of Akt1 induction in the skeletal muscle of the HF/HS-fed DTG mice (red, increase in concentration; blue, decrease in concentration) as compared with the controls fed the same diet. Increased Cori cycle activity and hepatic fatty acid oxidation were evident in the DTG mice. Abbreviations: α-KG, α-ketoglutarate; β-HB, β-hydroxybutyrate; DMG, dimethylglycine; G6P, glucose-6-phosphate; M6P, mannose-6-phosphate.

predominantly saturated, fatty acids can be synthesized in the liver from carbohydrate via de novo lipogenesis. Thus, in the DTG mice, it would appear that induction of AKT increases the oxidation of dietary derived fatty acids systemically and also stimulates the conversion of carbohydrate into shorter chain fatty acids in the liver. Intriguingly, these changes were less apparent in skeletal muscle, suggesting that a major part of the beneficial effect of AKT induction in skeletal muscle was initiated in the liver.

Tyynismaa and colleagues demonstrated that mitochondrial myopathy in skeletal muscle led to activation of Akt1 and induction of FGF-21.[32] In this study, the mice with late-onset mitochondrial myopathy exhibited smaller adipocytes and lower hepatic fat content and were resistant to weight gain on the high-fat diet. Collectively, these studies suggest that skeletal muscle could initiate molecular signaling and orchestrate systemic metabolic changes to reduce obesity.

CONCLUSIONS

In summary, a combination of ^{1}H NMR spectroscopy, GC−MS, GC−FID, and LC−MS was used to examine the metabolomic profiles of a conditional transgenic mouse model that specifically overexpresses the Akt1 gene in skeletal muscle. Our data indicate that Akt1 activation induced metabolic perturbations including upregulated anaerobic glycolysis in the gastrocnemius muscle as well as increased gluconeogenesis, glycogenolysis, and ketogenesis in the liver. These processes demonstrated how muscle hypertrophy can alter systemic metabolism, influencing distant organs, to supply nutrients required for myogenic cell growth and at the same time limit diet-induced obesity. Taken together, the current study highlights the metabolic role of glycolytic muscle fibers, which can be induced by resistance exercise, in regressing diet-induced obesity and age-related fat accumulation and improving glucose metabolism.

ASSOCIATED CONTENT

Supporting Information

Body weights of animals in the aging study at 12 weeks and 18 months, PCA scores plot of NMR spectra of gastrocnemius muscle tissue, sections of NMR spectra showing anserine and carnosine standards and a pooled gastrocnemius muscle extract mixed with D_2O or anserine standards, and summary of fatty acids changes due to induced genotype detected following analysis by GC−FID. This material is available free of charge via the Internet at http://pubs.acs.org.

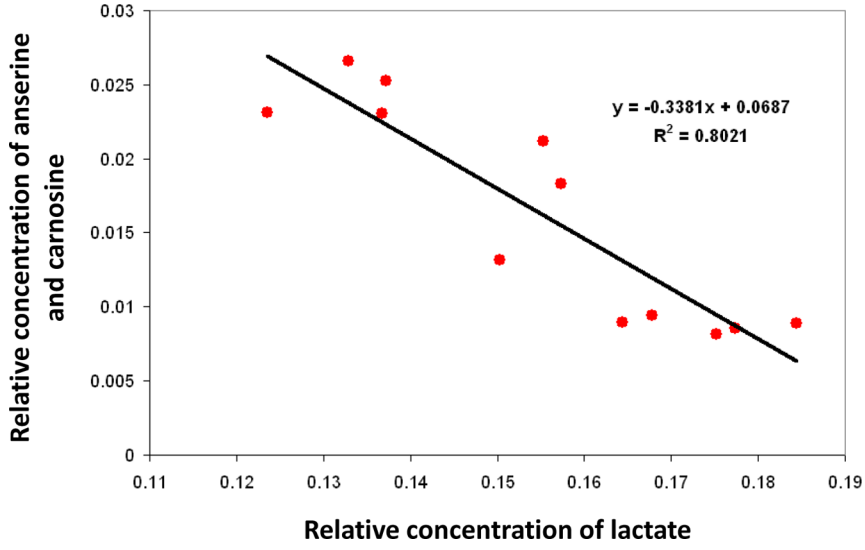

Figure 7. For the HF/HS-fed animals, the concentrations of anserine and carnosine were negatively correlated with the lactate concentration in the gastrocnemius muscle (Pearson correlation coefficient, $r = -0.90$). A weaker correlation was observed when all data from both diet and aging studies were considered ($r = -0.63$).

dx.doi.org/10.1021/pr500756u | J. Proteome Res. 2015, 14, 342−352

AUTHOR INFORMATION

Corresponding Author

*Tel.: +44 (0)1223 437503. Fax: +44 (0)1223 437515. E-mail: jules.griffin@mrc-hnr.cam.ac.uk.

Notes

The authors declare no competing financial interest.

ACKNOWLEDGMENTS

The authors gratefully thank the support from Universiti Teknologi Malaysia (K.-K.C.), the Royal Society, UK (J.L.G.), the Medical Research Council, UK (Lipid Profiling and Signalling programme grant; UD99999906; J.L.G.), the Wellcome Trust (UPLC QToF MS based lipidomics; 093148/Z/10/Z; J.L.G.), and the National Institutes of Health (AG034972, HL081587, HL116591, and HL120160; K.W.).

REFERENCES

(1) Brazil, D. P.; Hemmings, B. A. Ten years of protein kinase B signalling: a hard Akt to follow. *Trends Biochem. Sci.* **2001**, *26*, 657−664.

(2) Fayard, E.; Tintignac, L. A.; Baudry, A.; Hemmings, B. A. Protein kinase B/Akt at a glance. *J. Cell Sci.* **2005**, *118*, 5675−5678.

(3) Manning, B. D.; Cantley, L. C. AKT/PKB signaling: navigating downstream. *Cell* **2007**, *129*, 1261−1274.

(4) Sale, E. M.; Sale, G. J. Protein kinase B: signalling roles and therapeutic targeting. *Cell. Mol. Life Sci.* **2008**, *65*, 113−127.

(5) Hoffman, E. P.; Nader, G. A. Balancing muscle hypertrophy and atrophy. *Nat. Med.* **2004**, *10*, 584−585.

(6) Izumiya, Y.; Hopkins, T.; Morris, C.; Sato, K.; Zeng, L.; Viereck, J.; Hamilton, J. A.; Ouchi, N.; LeBrasseur, N. K.; Walsh, K. Fast/glycolytic muscle fiber growth reduces fat mass and improves metabolic parameters in obese mice. *Cell Metab.* **2008**, *7*, 159−172.

(7) Wan, M.; Easton, R. M.; Gleason, C. E.; Monks, B. R.; Ueki, K.; Kahn, C. R.; Birnbaum, M. J. Loss of Akt1 in mice increases energy expenditure and protects against diet-induced obesity. *Mol. Cell. Biol.* **2012**, *32*, 96−106.

(8) Akasaki, Y.; Ouchi, N.; Izumiya, Y.; Bernardo, B. L.; Lebrasseur, N. K.; Walsh, K. Glycolytic fast-twitch muscle fiber restoration counters adverse age-related changes in body composition and metabolism. *Aging Cell* **2014**, *13*, 80−91.

(9) Grill, M. A.; Bales, M. A.; Fought, A. N.; Rosburg, K. C.; Munger, S. J.; Antin, P. B. Tetracycline-inducible system for regulation of skeletal muscle-specific gene expression in transgenic mice. *Transgenic Res.* **2003**, *12*, 33−43.

(10) Shiojima, I.; Sato, K.; Izumiya, Y.; Schiekofer, S.; Ito, M.; Liao, R.; Colucci, W. S.; Walsh, K. Disruption of coordinated cardiac hypertrophy and angiogenesis contributes to the transition to heart failure. *J. Clin. Invest.* **2005**, *115*, 2108−2118.

(11) Salek, R.; Cheng, K.-K.; Griffin, J. The study of mammalian metabolism through NMR-based metabolomics. *Methods Enzymol.* **2011**, *500*, 337−351.

(12) Le Belle, J. E.; Harris, N. G.; Williams, S. R.; Bhakoo, K. K. A comparison of cell and tissue extraction techniques using high-resolution ^{1}H-NMR spectroscopy. *NMR Biomed.* **2002**, *15*, 37−44.

(13) Atherton, H. J.; Gulston, M. K.; Bailey, N. J.; Cheng, K.-K.; Zhang, W.; Clarke, K.; Griffin, J. L. Metabolomics of the interaction between PPAR-α and age in the PPAR-α-null mouse. *Mol. Syst. Biol.* **2009**, *5*, 259.

(14) Wishart, D. S.; Tzur, D.; Knox, C.; Eisner, R.; Guo, A. C.; Young, N.; Cheng, D.; Jewell, K.; Arndt, D.; Sawhney, S.; et al. HMDB: the Human Metabolome Database. *Nucleic Acids Res.* **2007**, *35*, D521−526.

(15) Nicholson, J. K.; Foxall, P. J.; Spraul, M.; Farrant, R. D.; Lindon, J. C. 750 MHz ^{1}H and ^{1}H−^{13}C NMR spectroscopy of human blood plasma. *Anal. Chem.* **1995**, *67*, 793−811.

(16) Gullberg, J.; Jonsson, P.; Nordström, A.; Sjöström, M.; Moritz, T. Design of experiments: an efficient strategy to identify factors influencing extraction and derivatization of *Arabidopsis thaliana* samples in metabolomic studies with gas chromatography/mass spectrometry. *Anal. Biochem.* **2004**, *331*, 283−295.

(17) Morrison, W. R.; Smith, L. M. Preparation of fatty acid methyl esters and dimethylacetals from lipids with boron fluoride−methanol. *J. Lipid Res.* **1964**, *5*, 600−608.

(18) Reilly, M. P.; Rader, D. J. The metabolic syndrome: more than the sum of its parts? *Circulation* **2003**, *108*, 1546−1551.

(19) Lai, K.-M. V.; Gonzalez, M.; Poueymirou, W. T.; Kline, W. O.; Na, E.; Zlotchenko, E.; Stitt, T. N.; Economides, A. N.; Yancopoulos, G. D.; Glass, D. J. Conditional activation of akt in adult skeletal muscle induces rapid hypertrophy. *Mol. Cell. Biol.* **2004**, *24*, 9295−9304.

(20) Holliday, R.; McFarland, G. A. Inhibition of the growth of transformed and neoplastic cells by the dipeptide carnosine. *Br. J. Cancer* **1996**, *73*, 966−971.

(21) Renner, C.; Asperger, A.; Seyffarth, A.; Meixensberger, J.; Gebhardt, R.; Gaunitz, F. Carnosine inhibits ATP production in cells from malignant glioma. *Neurol. Res.* **2010**, *32*, 101−105.

(22) Gariballa, S. E.; Sinclair, A. J. Carnosine: physiological properties and therapeutic potential. *Age Ageing* **2000**, *29*, 207−210.

(23) Holliday, R.; McFarland, G. A. A role for carnosine in cellular maintenance. *Biochemistry (Moscow)* **2000**, *65*, 843−848.

(24) Maemura, H.; Goto, K.; Yoshioka, T.; Sato, M.; Takahata, Y.; Morimatsu, F.; Takamatsu, K. Effects of Carnosine and Anserine Supplementation on Relatively High Intensity Endurance Performance. *Int. J. Sport Health Sci.* **2006**, *4*, 86−94.

(25) Jia, H.; Qi, X.; Fang, S.; Jin, Y.; Han, X.; Wang, Y.; Wang, A.; Zhou, H. Carnosine inhibits high glucose-induced mesangial cell proliferation through mediating cell cycle progression. *Regul. Pept.* **2009**, *154*, 69−76.

(26) Renner, C.; Zemitzsch, N.; Fuchs, B.; Geiger, K. D.; Hermes, M.; Hengstler, J.; Gebhardt, R.; Meixensberger, J.; Gaunitz, F. Carnosine retards tumor growth in vivo in an NIH3T3-HER2/neu mouse model. *Mol. Cancer* **2010**, *9*, 2.

(27) Carpten, J. D.; Faber, A. L.; Horn, C.; Donoho, G. P.; Briggs, S. L.; Robbins, C. M.; Hostetter, G.; Boguslawski, S.; Moses, T. Y.; Savage, S.; et al. A transforming mutation in the pleckstrin homology domain of AKT1 in cancer. *Nature* **2007**, *448*, 439−444.

(28) Ju, X.; Katiyar, S.; Wang, C.; Liu, M.; Jiao, X.; Li, S.; Zhou, J.; Turner, J.; Lisanti, M. P.; Russell, R. G.; et al. Akt1 governs breast cancer progression in vivo. *Proc. Natl. Acad. Sci. U.S.A.* **2007**, *104*, 7438−7443.

(29) Liu, H.; Radisky, D. C.; Nelson, C. M.; Zhang, H.; Fata, J. E.; Roth, R. A.; Bissell, M. J. Mechanism of Akt1 inhibition of breast cancer cell invasion reveals a protumorigenic role for TSC2. *Proc. Natl. Acad. Sci. U.S.A.* **2006**, *103*, 4134−4139.

(30) Izumiya, Y.; Bina, H. A.; Ouchi, N.; Akasaki, Y.; Kharitonenkov, A.; Walsh, K. FGF21 is an Akt-regulated myokine. *FEBS Lett.* **2008**, *582*, 3805−3810.

(31) Xu, J.; Lloyd, D. J.; Hale, C.; Stanislaus, S.; Chen, M.; Sivits, G.; Vonderfecht, S.; Hecht, R.; Li, Y.-S.; Lindberg, R. A.; et al. Fibroblast growth factor 21 reverses hepatic steatosis, increases energy expenditure, and improves insulin sensitivity in diet-induced obese mice. *Diabetes* **2009**, *58*, 250−259.

(32) Tyynismaa, H.; Carroll, C. J.; Raimundo, N.; Ahola-Erkkilä, S.; Wenz, T.; Ruhanen, H.; Guse, K.; Hemminki, A.; Peltola-Mjøsund, K. E.; Tulkki, V.; et al. Mitochondrial myopathy induces a starvation-like response. *Hum. Mol. Genet.* **2010**, *19*, 3948−3958.